Properties of neutron emission in fission processes induced by ^{20}Ne+^{159}Tb and ^{20}Ne+^{169}Tm reactions between $E=8$ and 16 MeV/nucleon

Th. Keutgen, J. Cabrera, Y. El Masri, Ch. Dufauquez, V. Roberfroid, I. Tilquin, A. Ninane, and J. Van Mol
FNRS and Institute of Nuclear Physics, Université Catholique de Louvain, B-1348 Louvain-la-Neuve, Belgium

R. Régimbart
Laboratoire de Physique Corpusculaire, IN2P3, CNRS/ISMRA, F-14050 Caen Cedex, France

R. J. Charity
Department of Chemistry, Washington University, St. Louis, Missouri 63130, USA

J. B. Natowitz, K. Hagel, and R. Wada
Cyclotron Institute, Texas A&M University, College Station, Texas 77845, USA

D. J. Hinde
Department of Nuclear Physics, The Australian National University, Canberra, Australia
(Received 2 October 2003; revised manuscript received 18 May 2004; published 29 July 2004)

Neutron emission in $E=8$, 10, 13, and 16 MeV/nucleon ^{20}Ne+^{159}Tb, ^{169}Tm induced fission reactions has been further studied. The 4π configuration of the DEMON neutron multidetector allowed a detailed investigation of the pre- and postscission properties as functions of the fission parameters. The emission of the neutrons from their respective sources was found to be isotropic to a high degree. The determination of the compound-nucleus recoil velocity and the kinetic-energy release in fission suffers from smearing due to the recoil kicks imparted by the evaporated pre- and postscission light particles. Attempts to gate on these quantities lead to biases in the emission patterns of the evaporated neutrons. Specifically, with such gates, the assumption of isotropic emission is violated and attempts to analyze such gated neutron spectra with the standard fitting technique, which assumes isotropy, lead to spurious results. All these effects are clearly illustrated in this work.

DOI: 10.1103/PhysRevC.70.014611 PACS number(s): 25.70.Jj, 25.85.Ge

I. INTRODUCTION

The study of neutron emission accompanying statistical fission has highlighted the important role of dynamics and dissipation in fission-evaporation competition [1]. Recently we have reported on neutron and light charged particle emission in $E=8$, 10, 13, and 16 MeV/nucleon ^{20}Ne+^{159}Tb, ^{169}Tm induced fission reactions [2]. At the lowest bombarding energy, the fission process is entirely statistical and associated with complete fusion. At the higher bombarding energies, the fission yield has increasing contributions from the fast-fission process and the fraction of the projectile's linear momentum transferred to the fused system decreases.

Due to their neutral charge, neutrons are not sensitive to the Coulomb field and thus, typically display much higher multiplicities than the competing light charged particles in the decay of highly excited and rotating nuclei. In the study of fission dynamics, neutrons detected in coincidence with fission fragments (FF) are assumed to originate from up to four moving sources. In temporal order, the first emitted are the preequilibrium neutrons (PE) with multiplicity (ν_n^{PE}), second are the prescission neutrons evaporated from the compound nucleus (CN) prior to scission (ν_n^{CN}), and last are the postscission neutrons evaporated from the two fission fragment sources (ν_n^{F1} and ν_n^{F2}). In our experiments, the PE neutron contribution was proportionately very weak as compared to the contributions of the other neutron sources. However, the properties of this contribution have been made the object of a very detailed discussion in Ref. [2]. Therefore, in the following, we will concentrate on the discussion of the properties of the neutrons emitted by the three other sources and invite the reader to refer to the previously reported analysis [2].

The present paper aims to extend the analysis of these previously reported data [2]. By analyzing the in-plane and out-of-plane anisotropy of the neutron emission and the dependence of the extracted multiplicities on the fission mass partition, the extent to which meaningful multiplicities can be deduced as functions of the total kinetic-energy release in fission, TKE, and the CN recoil velocity (V_{CN}) will be investigated [3].

In Sec. II, some details on the experimental setup and the data analysis procedures are given. In Sec. III, the neutron properties associated with different fission-fragment mass partitions are discussed. The effects of the CN recoil velocity and fission fragment TKE on the neutron angular distributions are presented in Sec. IV. This section will lead to a discussion, in Sec. IV C, concerning the anisotropy of the neutron emission in and out of the reaction plane. The conclusion of this work is contained in Sec. V.

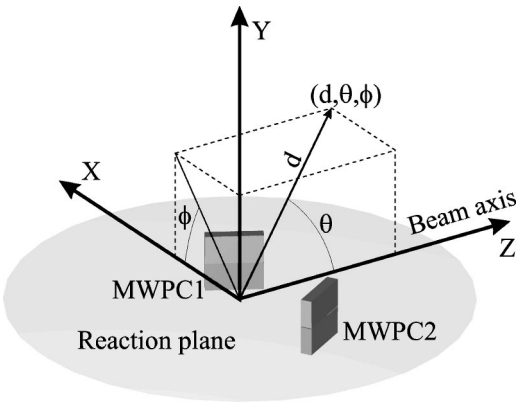

FIG. 1. Schematic showing the reaction plane and the definition of the distance d, θ and ϕ angles used for the positioning of the detectors in and out of the reaction chamber. The target is taken as the origin of the reference system and the beam direction as the z axis.

II. DETAILS ON THE EXPERIMENTAL SETUP AND PROCEDURES OF THE DATA ANALYSIS

This study was performed at the Louvain-la-Neuve cyclotron facility. Beams of ^{20}Ne were delivered at energies of $E=8$, 10, 13, and 16 MeV/nucleon and used to bombard targets of ^{159}Tb and ^{169}Tm. Both targets were 250 ± 8 μg/cm^2 thick.

The experimental setup has been detailed in Ref. [2]. Briefly, we recall that coincident FF issuing from the reactions were detected in two, 20×20 cm^2, X and Y position sensitive multiwire proportional gas counters (MWPC1 and MWPC2). The emission directions of the detected fragments were determined in both the polar and the azimuthal angles (θ,ϕ) with respect to the beam axis while each counter subtended up to 40° opening angles in the two directions. The two MWPCs were arranged symmetrically on each side of the beam axis as shown in Fig. 1. Their central angular positions θ_{MWPC} (around +67° and −67°) were adjusted for each beam energy to optimize the coincidence rate and especially to cover in coincidence the entire FF mass distributions.

Neutrons emitted in coincidence with the FFs were detected in the 81 DEMON, NE213 liquid-scintillator counters, each consisting of an active volume of 16 cm diameter by 20 cm thickness. These detectors were mounted at a distance of flight of 185 cm from the target and were arranged in a 4π geometry as shown in Fig. 3 of Ref. [2]. The reaction chamber was located at a distance of 5 m above the ground of the cyclotron target hall. The n-γ discrimination technique and the intrinsic detection efficiency of the DEMON cells as functions of neutron energy and electronic detection thresholds have been discussed in great detail in Ref. [4].

The DEMON detectors were supported on a lightweight Al structure offering several geometrical symmetries with respect to the frame system displayed in Fig. 1 as shown in Table I. Thus, for example, in the horizontal reaction plane defined by $\phi_n=0°$ and $\phi_n=180°$, there were 2×9 detectors set at 12.5°, 30°, 50°, 70°, 90°, 110°, 130°, 150°, and 167.5°. In the planes defined by $\phi_n=22.5°$ and 202.5° there were 2 $\times3$ detectors placed at $\theta_n=70°$, 90°, and 110° and so on. As the target was set perpendicularly to the beam axis for the measurements in this work, all the $\theta_n=90°$ detectors viewed the target through its thick metallic holder frame. Similarly, many of the DEMON detectors were totally or partially hidden from the target by the vacuum pumping system, massive detectors set in the reaction chamber, screws. These detectors were excluded from this study (they are marked by stars in Table I).

TABLE I. List of the central θ_n and ϕ_n angular positions of the 81 DEMON detectors positioned at 185 cm distance of flight from the target. Each detector is designated by a number, where detectors with the same first digit have the same value of θ_n. The detectors placed at 90° perpendicularly to the beam axis or hidden from the target by massive material set in the reaction chamber are designated by stars. Their data were excluded from this study.

θ_n(°) / ϕ_n(°)	12.5	30	50	70	90	110	130	150	167.5
337.5				610*	510*	410			
330			708*				308		
315		806						206	
300			709				309		
292.5									
270	904*	807*	710*				310*	207*	104*
247.5									
240			711				311		
225		808						208	
210			712*				312		
202.5				616*	516*	416			
180	901*	801	701	601	501*	401	301	201	101
157.5				602*	502*	402			
150			702*				302		
135		802		603	503*	403		202	
120			703				303		
112.5				604	504*	404			
90	902	803	704	605	505*	405	304	203	102
67.5				606	506*	406			
60			705				305		
45		804		607	507*	407		204	
30			706*				306		
22.5				608*	508*	408			
0	903*	805*	707	609	509*	409	307	205	103

The neutron kinetic-energy spectra were constructed from measured neutron times of flight and corrected for the energy-dependent intrinsic neutron detection efficiency [4]. The spectra were normalized to their solid angles and the number of triggering FFs [5]. All double-differential multiplicity spectra $d^2\nu_n/d\Omega dE_n$ (often designated in the following by double differential neutron energy spectra) from each DEMON detector were fitted by a single theoretical function. This function consists of the sum of four components, each associated with a particular neutron source that emits isotropically in its rest frame. The sources are the preequilibrium

neutron source PE, the CN, and the two fission fragments F1 and F2. The emission spectrum from the CN was assumed to be a "surface" type Maxwellian distribution [2]. Its expression in the laboratory system is

$$f_S(T_n,\nu_n)=\frac{\nu_n}{4\pi T_n^2}\sqrt{E_n\overline{E_n}}e^{-(\overline{E_n}/T_n)}, \tag{1}$$

while the spectra associated with the FFs and the PE were assumed to be a "volume" type, or a Watt distribution [2]. Its expression in the laboratory system is

$$f_V(T_n,\nu_n)=\frac{\nu_n}{2(\pi T_n)^{3/2}}\sqrt{E_n}e^{-(\overline{E_n}/T_n)}. \tag{2}$$

In these equations, ν_n and T_n are the multiplicities and the effective temperatures associated with the different sources, respectively,

$$\overline{E_n}=E_n+\tfrac{1}{2}m_n v_s^2-v_s\sqrt{2m_nE_n}\cos\,\alpha_R, \tag{3}$$

where E_n and $\overline{E_n}$ are the neutron energies in the laboratory and in the center-of-mass frames, respectively. v_s is the velocity of the emitting source, m_n is the neutron mass, and α_R is the relative angle between the direction of the emitting source and the direction of the detected neutron. With (θ,ϕ), the polar and azimuthal angles of the source, and (θ_n,ϕ_n), the corresponding angles of the DEMON detectors, one can write

$$\cos(\alpha_R)=\sin(\theta_n)\sin(\theta)\cos(\phi_n-\phi)+\cos(\theta_n)\cos(\theta). \tag{4}$$

Therefore, the function used to fit the neutron energy distributions, detected in coincidence with the two FFs in the MWPCs, was

$$\frac{d^2\nu_n}{d\Omega dE_n}=f_S(T_n^{\mathrm{CN}},\nu_n^{\mathrm{CN}})+f_V(T_n^{\mathrm{F1}},\nu_n^{\mathrm{F1}})+f_V(T_n^{\mathrm{F2}},\nu_n^{\mathrm{F2}})+f_V(T_n^{\mathrm{PE}},\nu_n^{\mathrm{PE}}), \tag{5}$$

where T_n^{CN} and ν_n^{CN} are the effective temperature of the CN source (assumed to recoil along the beam axis) and the associated neutron multiplicity (prescission parameters); T_n^{F1} and ν_n^{F1} are the effective temperature of the F1 fission fragment detected in the MWPC1 and the associated neutron multiplicity (postscission parameters); T_n^{F2} and ν_n^{F2} are the effective temperature of the F2 fission fragment detected in the MWPC2 and the associated neutron multiplicity (postscission parameters); T_n^{PE} and ν_n^{PE} are "the effective temperature parameter" of the PE source and the associated neutron multiplicity.

In all cases the effective temperatures do not represent the initial temperatures of any of the sources, but they do describe the shape of the kinetic-energy spectra for each component. The PE emissions are not thermal at all and the effective temperature in this case is just a fitting parameter. The other sources are thermal, but contain multichance emissions each associated with decreasing nuclear temperatures as the system cools. The effective temperature can be related to the initial nuclear temperature t through statistical-model calculations. For example, assuming a constant level density parameter and no charged particle competition, LeCouteur and Lang [6,7] have shown that the effective temperature is proportional to the initial nuclear temperature, i.e., $T=\frac{11}{12}t$. At scission, the fission fragments are expected to be at thermal-equilibrium, i.e., $t^{\mathrm{F1}}=t^{\mathrm{F2}}$ and thus, assuming a proportional relation between T and t, independent of the nucleus mass, $T_n^{\mathrm{F1}}=T_n^{\mathrm{F2}}$. Therefore with this extra requirement, the nominal eight free parameters in the fit can be reduced to seven. These parameters were initially determined by fitting the double-differential neutron multiplicity spectra $d^2\nu_n/d\Omega dE_n$ for the whole set of DEMON detectors.

Subsequently, in a second fit step, the effective temperatures were held fixed and the multiplicity values were refined by fitting the neutron angular distributions $d\nu_n/d\Omega$ in and out of the reaction plane using the following expression

$$\left.\frac{d\nu_n}{d\Omega}\right|_{E_s}=\int_{E_s}^{\infty}f_S(T_n^{\mathrm{CN}},\nu_n^{\mathrm{CN}})dE_n+\int_{E_s}^{\infty}f_V(T_n^{\mathrm{F1}},\nu_n^{\mathrm{F1}})dE_n+\int_{E_s}^{\infty}f_V(T_n^{\mathrm{F2}},\nu_n^{\mathrm{F2}})dE_n+\int_{E_s}^{\infty}f_V(T_n^{\mathrm{PE}},\nu_n^{\mathrm{PE}})dE_n, \tag{6}$$

where $E_s=2$ MeV is the neutron energy threshold imposed on each experimental neutron spectrum (in our setup, neutrons and γ rays were already well discriminated above 1.25 MeV threshold). The Watt function is analytically integrable giving the following expression

$$\left.\frac{d\nu_n}{d\Omega}\right|_{E_s}=\int_{E_s}^{\infty}f_V(T^i{}_n,\nu_n^i)dE_n=\frac{\nu_n^i}{2\pi^{3/2}}\exp\left(\alpha_i^2-\frac{1}{T_n^i}\frac{E_i}{A_i}\right)\times\left\{\sqrt{\pi}\left(\alpha_i^2+\tfrac{1}{2}\right)[1-\mathrm{erf}(c_i)]+(2\alpha_i+c_i)\exp(-c_i^2)\right\}, \tag{7}$$

where $\alpha_i=\sqrt{(1/T^i{}_n)(E_i/A_i)}\cos\alpha_{Ri}$, $c_i=\sqrt{(E_s/T^i{}_n)}-\alpha_i$ and $\mathrm{erf}(c_i)$ the error function. E_i/A_i is the kinetic energy per nucleon of the considered emitting source (i=F1, F2 or PE). In contrast, the Maxwellian function had to be numerically integrated.

The velocities of the two FF sources were fixed to their mean velocities measured with MWPC1 and MWPC2 for a given mass partition while the velocity of the CN prescission source was fixed to the mean value of V_{CN} obtained from the experimentally measured evaporation residue velocity distributions [2]. One must remember that these velocities are not equal to the reaction center-of-mass velocities (V_{cm}) because of incomplete linear momentum transfer due to the occurrence of incomplete fusion or preequilibrium processes. The PE source was assumed to move with the half of the beam velocity [2,8].

Examples of some of the many fitted spectra and the corresponding angular distributions both in and out of the reaction plane (defined by $\phi_n=0°$ and 180°) are shown in Figs. 2 and 3 for the $E=10$ MeV/nucleon reaction on the ^{169}Tm

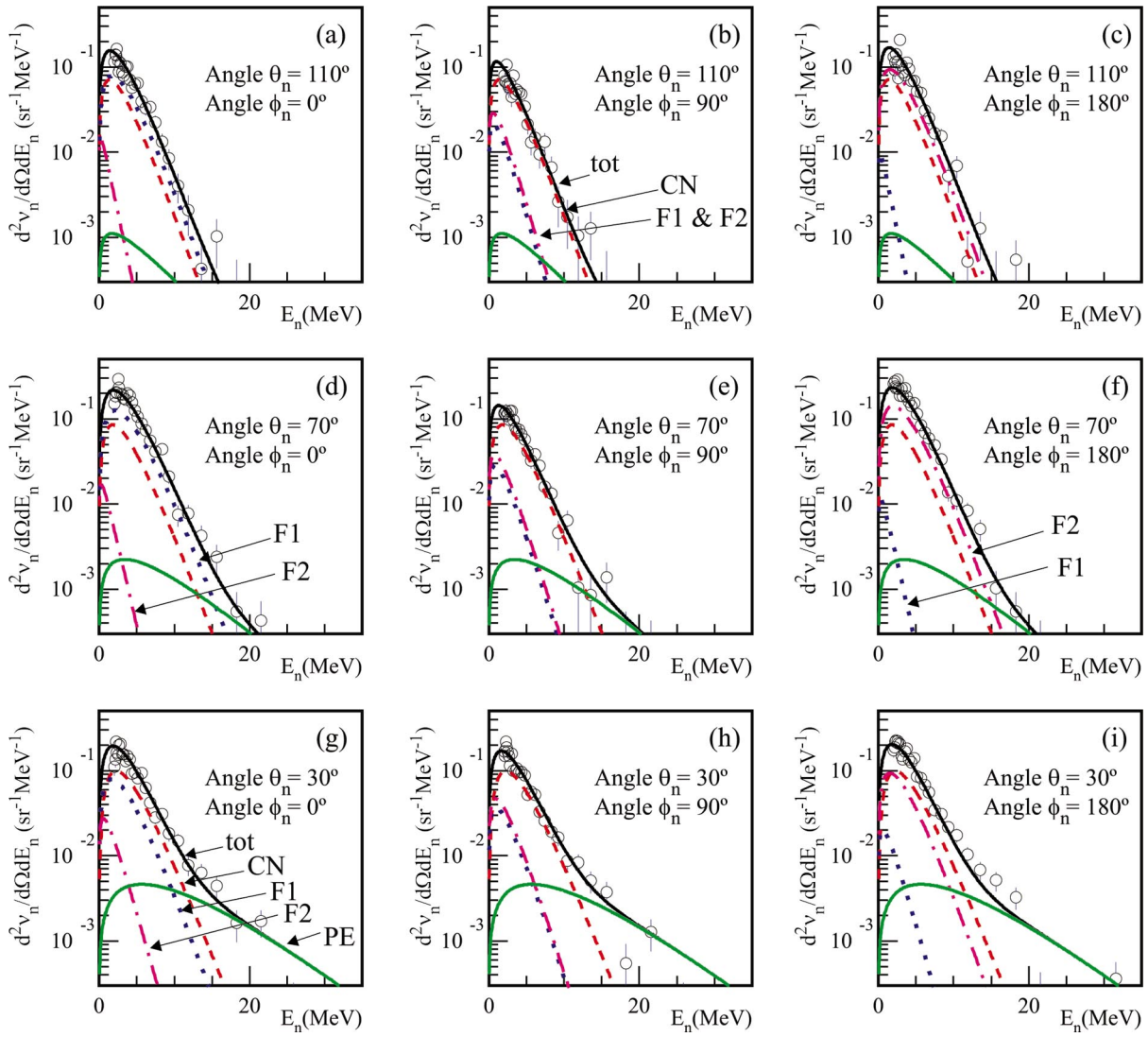

FIG. 2. (Color) Some examples of the multiple-moving-source fits (curves) to the experimental neutron kinetic-energy spectra (open circles and their error bars) for symmetric fission partition in the laboratory frame for the $E=10$ MeV/nucleon ^{20}Ne+^{169}Tm reaction. The thick curves (tot) indicate the total contributions from all sources. The contributions from each of the sources are indicated by the labeled curves; (CN) for the prescission CN source, (F1) and (F2) for the two fission fragments, and (PE) for the preequilibrium emission.

target and for symmetric fission partition $[A_{F1}=A_{F2}=(A_{CN}/2)\pm 5$ nucleons]. The spectra in Figs. 2(d) and 2(f) are for the DEMON detectors set directly behind MWPC1 and MWPC2, respectively. Due to the kinematic focusing of the postscission neutrons by the FFs, these spectra are dominated by the contributions from the respective fission fragments (F1 and F2). The PE component is constrained largely from the most forward-angle DEMON detectors set at 12.5° and 30° [Fig. 2(g)]. The extracted PE multiplicities have been discussed in Ref. [2] and are listed in Table IV in that reference.

It is important for the following, to notice that the spectra for DEMON detectors set at backward angles have the largest contributions from the CN source as shown in Fig. 2(b). In Fig. 3, the simultaneous fit to all of the experimental angular distributions both in and out of the reaction plane, is extremely good. This indicates that the data are generally well described by these four moving sources with the assumption of an isotropic neutron emission in the rest frame of the emitting nuclei. Completely identical conclusions can also be drawn from the analysis of the data obtained with the ^{159}Tb target [2].

III. NEUTRON-MULTIPLICITY DISTRIBUTIONS AS A FUNCTION OF FISSION-FRAGMENT MASS PARTITION

Figure 4 shows the fitted neutron multiplicities and the effective temperatures as a function of the fission-fragment mass A_{F1}. The results are shown for both targets (Tm and Tb) at the four ^{20}Ne beam energies. In this figure, we have considered bin widths of ±5 nucleons around the displayed values on the mass axis. The solid data points (triangles and circles corresponding to the Tb and Tm targets, respectively)

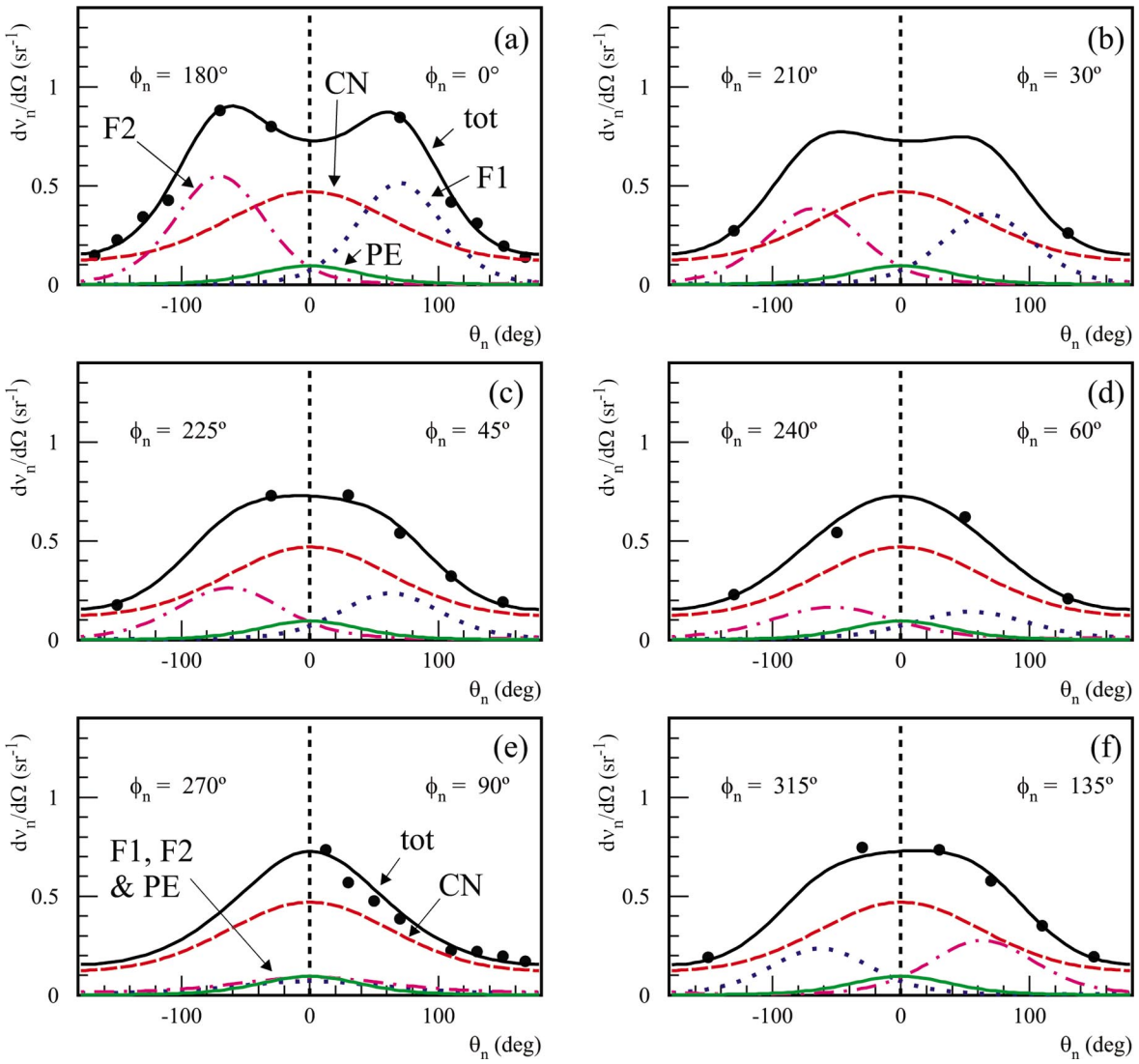

FIG. 3. (Color) Examples of some of the multiple-moving-source fits (curves) to the experimental neutron θ_n distributions (solid circles) $E=10$ MeV/nucleon ^{20}Ne+^{169}Tm reaction. Results shown are the distributions plotted in the laboratory frame for the symmetric fission partition. Distributions both in ($\phi_n=0°,180°$) and others at different ϕ_n angles to the reaction plane are shown. The curves have the same meaning as in Fig. 2 and the fits correspond to the same set of fitted parameters (ν^i, T^i) as those in Fig. 2.

are associated with the fitted prescission neutron results ν_n^{CN}, while the open data points are associated with ν_n^{FF}. In Ref. [2], we have already stressed the similarity of the results for the two targets. This is not surprising as the target masses are only 7% different. In fact, the most important observed difference between the two systems is in the evaporation residue (ER) formation cross section, which is higher for the lighter system as shown and discussed in Ref. [2].

The experimentally extracted prescission neutron multiplicity has been fitted by a parabolic function:

$$f(p_0,p_1) = p_1 + p_0\left(A_{\mathrm{F1}} - \frac{A_{\mathrm{CN}}}{2}\right)^2, \tag{8}$$

where $A_{\mathrm{CN}}/2$ is the FF mass in case of symmetric partition, p_0 and p_1 are the free parameters for the fit. p_0 is the important parameter for the determination of the FF mass-dependence of the multiplicity. The more p_0 differs from zero, the larger is the dependence of the multiplicity on mass split. In Fig. 4, prescission data from all bombarding energies were simultaneously fitted with a common p_0 value. The fitted values are $p_0=(-6.7\pm1.2)10^{-4}$ and $(-10.3\pm1.9)10^{-4}$ for the Tm and Tb targets, respectively, and thus there is a small but statistically significant A_{F1} dependence. In practice, p_0 might depend on bombarding energy, but the statistical errors obtained from individually fitting each bombarding energy were too large to make any conclusion. The postscission multiplicities increases almost linearly with A_{F1}. The effective temperatures do not show any significant dependence on the FF mass partition. The linear dependence of the postscission multiplicities is consistent with a mass-partition-independent effective temperature for the postscission emissions. Assuming initial fission-fragment excitation energy (U_{F1}) proportional to the square of the effective temperature, one finds

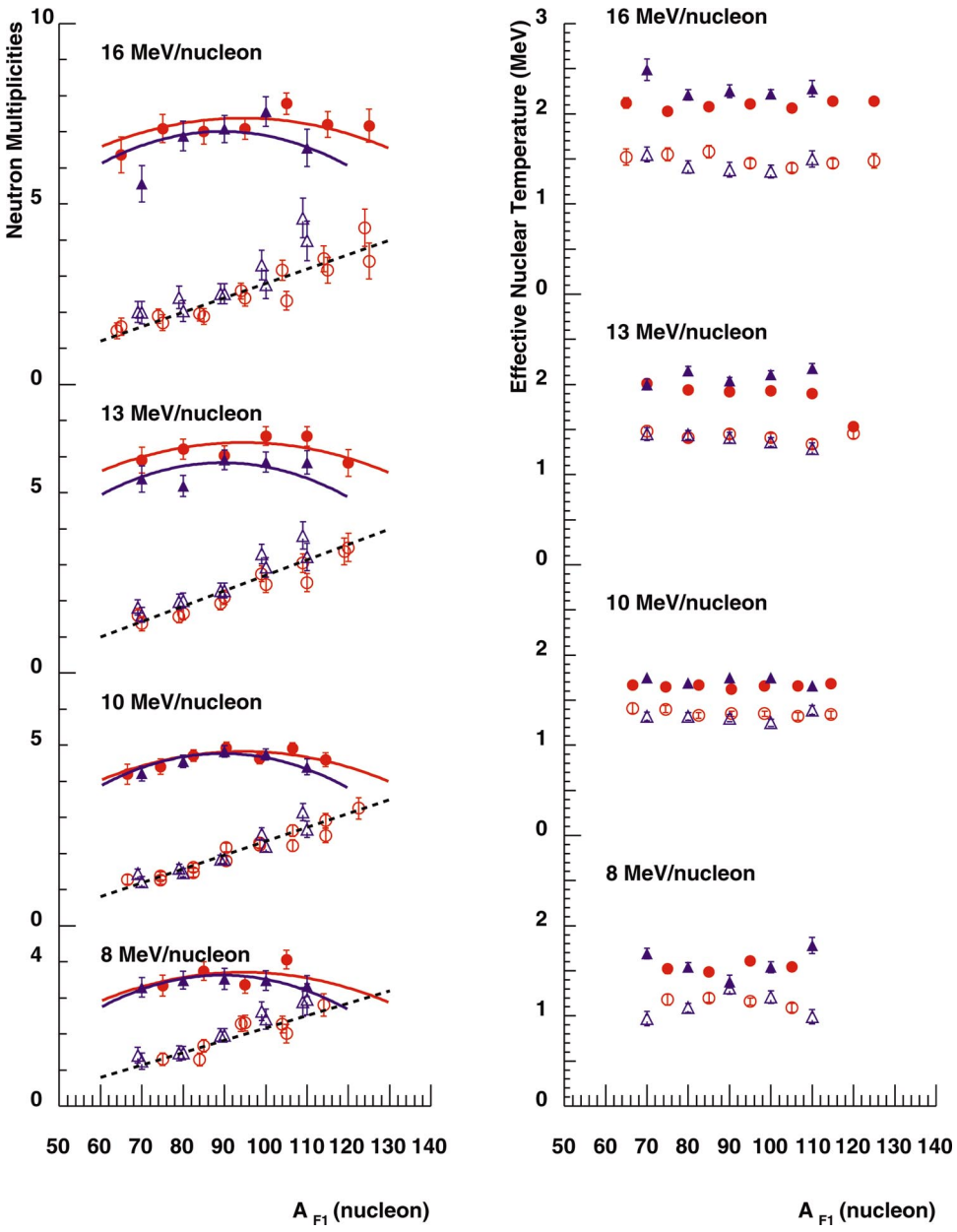

FIG. 4. (Color) Evolutions of the ν_n^{CN} (solid symbols) and ν_n^{FF} (open symbols) neutron multiplicities and the corresponding effective temperatures as a function of fission fragment mass, A_{F1}, for the two reactions studied. The triangular symbols represent results obtained with the Tb target (blue color) while the circular symbols depict those obtained with the Tm target (red color). The dashed lines are to guide the eye. The full line results from parabolic fits (see test for details).

$$U_{F1} \propto a_n (T_n^{F1})^2 = \frac{A_{F1}}{a_0} (T_n^{F1})^2, \tag{9}$$

where a_n is the level-density parameter and a_0, the level-density constant (varying from 8 to 13 MeV as a function of the temperature). As $T_n^{F1}$is mass-partition independent within the experimental uncertainties and the neutron multiplicity is roughly proportional to U_{F1}, then this multiplicity becomes approximately proportional to A_{F1} even if a_0 is temperature dependent.

Figure 5 shows the evolution of the total neutron multiplicities $\nu_n^{tot} = \nu_n^{CN} + \nu_n^{F1} + \nu_n^{F2}$ as well as $\nu_n^{post} = \nu_n^{F1} + \nu_n^{F2}$ as a function of the FF mass partition. The total multiplicities are almost independent of the FF mass within the experimental uncertainties [fits with Eq. (8) give $p_0 = (-3.9 \pm 1.4)10^{-4}$ and $(2.9 \pm 3.3)10^{-4}$ for the Tm and Tb reactions, respectively]. The total neutron multiplicity is related to the excitation energy available for evaporation [9], which is the total excitation energy minus the Q value for fission (Q_f) and TKE. The quantities Q_f and TKE have opposite dependencies on mass partition and if they cancel, ν_n^{tot} shows a flat distribution as a function of A_{F1}. However, this behavior can be system dependent. For the reactions studied in this paper, systematic (Q_f − TKE) values [using the liquid drop model and TKE from Eq. (11)] were calculated as a function of the FF mass partition and a maximum of around 5 MeV difference was found between the symmetric and the most asymmetric measured mass partition. This difference in (Q_f − TKE) suggests less than 0.5 neutron difference in the total neutron multiplicity. Consequently, we do not expect a strong dependence in our reactions.

The dependencies of these fitted neutron parameters on mass partition have been reported in a number of previous studies covering a range of heavy-ion induced fission reac-

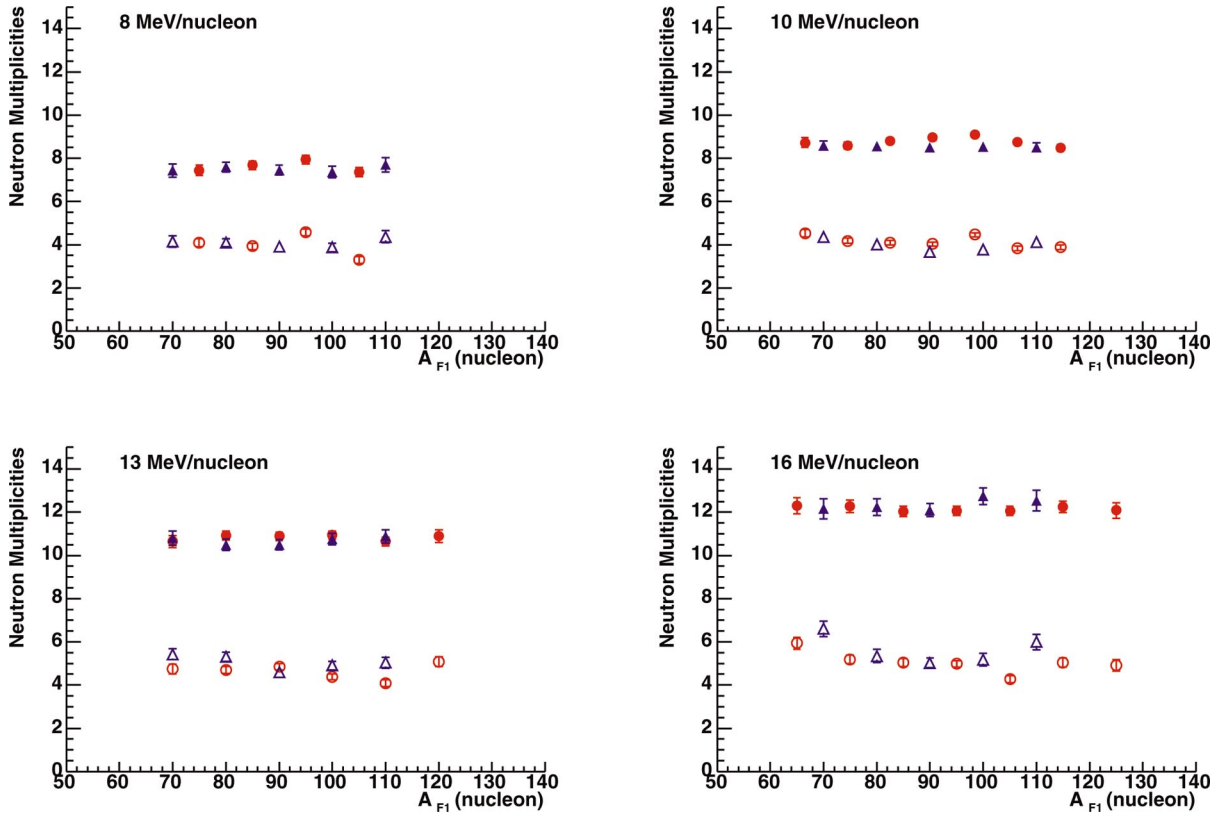

FIG. 5. (Color) Evolutions of the total neutron multiplicities ν_n^{tot} (solid symbols) and ν_n^{post} (open symbols) as a function of fission-fragment mass A_{F1}. The triangular and circular data points are for the Tb and Tm targets, respectively.

tions [3,10,11]. All report the nearly linear rise of the postscission multiplicities with fragment mass. The $E=5.7$ MeV/nucleon ^{36}Ar+^{169}Tm reaction, studied in Ref. [11], showed no measurable dependence of the prescission multiplicity with mass partition. The same is true for the $E=5.5$ and 6.3 MeV/nucleon ^{19}F+^{232}Th reactions studied in Ref. [10], though the sensitivity may be limited due to the contamination of the fusion-fission yield with nucleon transfer fission. The presaddle neutron multiplicities from these two studies were fitted with Eq. (8) and give values of $p_0=(1\pm5)10^{-4}$ and $(-0.4\pm3.8)10^{-4}$, respectively. In Ref. [3], Hinde *et al.* report a measurable dependence of mass partition for a range of reactions including the $E=8.8$ MeV/nucleon ^{18}O+^{154}Sm reaction which is quite similar to the Ne+Tb reaction studied in this work. Our fit to this O+Sm data set gives $p_0=(-14\pm4)10^{-4}$ and this is certainly consistent with the value we obtained with the Tb target. However, all p_0 values extracted from this and the referenced studies are consistent within two standard deviations. Clearly more systematic studies are needed to better constrain the mass-asymmetry dependence of the presaddle neutron multiplicity.

Statistical-model calculations with constant mass-asymmetry-independent presaddle delay times do not produce a mass-partition dependence of the presaddle multiplicities [12]. Thus if the A_{F1} dependence for ν_n^{CN} is larger than that for ν_n^{tot}, it suggests that the dynamical times, either presaddle and/or saddle-to-scission times, are dependent on mass partition. Our data suggest this (p_0 for ν_n^{CN} is larger than the value for ν_n^{tot}), but this is only a two standard deviation effect, so the statistical significance is not great. In a broad sense, such a dependence is not unexpected if fission and evaporation are considered part of a common binary-decay mode [3]. As no dynamical decays are generally associated with evaporation, a reduction in dynamical time is expected as we approach the extremely asymmetric evaporative binary decays.

Finally, while the mean (over FF masses) prescission neutron multiplicities increase almost linearly (from 4.2 to 8.3) with CN excitation energy (from 108 to 254 MeV) independently of the FF mass partition, the ν_n^{post} appear to saturate around a mean value of 4.2 (mean value over the FF masses and for the different bombarding energies) starting already at $\sim$100 MeV excitation energy (see also [2]). This saturation may even start at lower E^* value [13]. This confirms that nuclear fission is a cold process occurring at very low excitation energy and apparently independent of the initial excitation energy of the fissioning nuclei at least above a given threshold ($<$100 MeV).

IV. EFFECTS OF THE CN RECOIL VELOCITY ON THE NEUTRON ANGULAR DISTRIBUTION

A. CN recoil velocity distribution

In many previous studies [14–17], the contributions of the incomplete fusion process to the detected fission events were accounted for by performing specific selections (cuts) on the

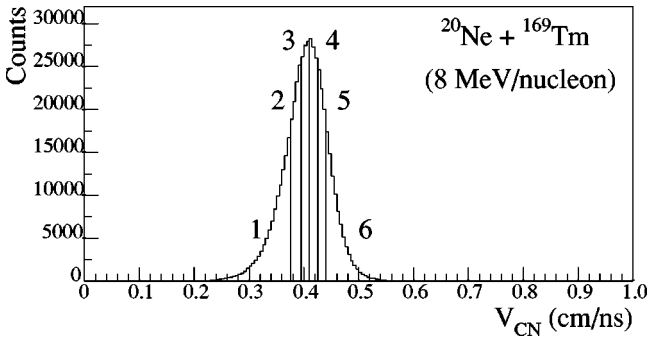

FIG. 6. Experimental CN recoil velocity distribution V_{CN} for the $E=8$ MeV/nucleon ^{20}Ne+^{169}Tm reaction. This distribution corresponds to the entire fission mass partition. The vertical lines delimit the different bin cuts performed on this distribution in order to illustrate the CN recoil-velocity effects on the neutron angular distributions (see text for details).

CN recoil-velocity distributions. Incomplete fusion is normally characterized by an incomplete transfer of the projectile's linear-momentum to the CN. Consequently, the CN recoil velocity is expected to be lower than that for complete fusion, in which there is a full momentum transfer. In this work, the $E=10$, 13, and 16 MeV/nucleon reactions show mean CN velocities smaller than the complete fusion values and thus this indicates incomplete-fusion reactions are present [2]. For reactions like these and others for which both complete and incomplete fusion reactions may be mixed, if one wants to experimentally reject the events associated with incomplete fusion, a selection on the highest CN recoil velocities might well be thought to be sufficient (Refs. [14,15]). Alternatively, for reactions with a wide range of momentum transfers, gating on the different recoil velocities will give an excitation-energy dependence (Refs. [16,17]). We will show in this section and the following, that such selections on the recoil velocity should be applied with a very great care.

The CN recoil velocity along the beam axis can be extracted from the measured FF velocities (V_{Fi}) and their detection angles (θ_i) as

$$V_{CN} = \frac{V_{F1}V_{F2}\,\sin(\theta_1+\theta_2)}{V_{F1}\,\sin(\theta_1)+V_{F2}\,\sin(\theta_2)}. \qquad (10)$$

This distribution for the $E=8$ MeV/nucleon ^{20}Ne+^{169}Tm reaction is shown in Fig. 6. It is associated with the entire fission mass distribution. This reaction was specifically chosen because no significant contribution from incomplete fusion is expected to be present. Effectively, in this reaction, both the ER velocity distribution and the fission-fragment folding-angle distribution are consistent with full linear-momentum transfer [2]. As such, the CN recoil-velocity should be single valued or with a small width due to the time resolution of the detectors. We measured a distribution with a larger width in Fig. 6 because Eq. (10) does not take into account the recoil kicks induced by the evaporation of pre- and postscission light particles. As long as these emissions are isotropic (in the rest frame of the emitting fragments), the centroids of the V_{CN} distributions are unaffected, so Eq. (10)

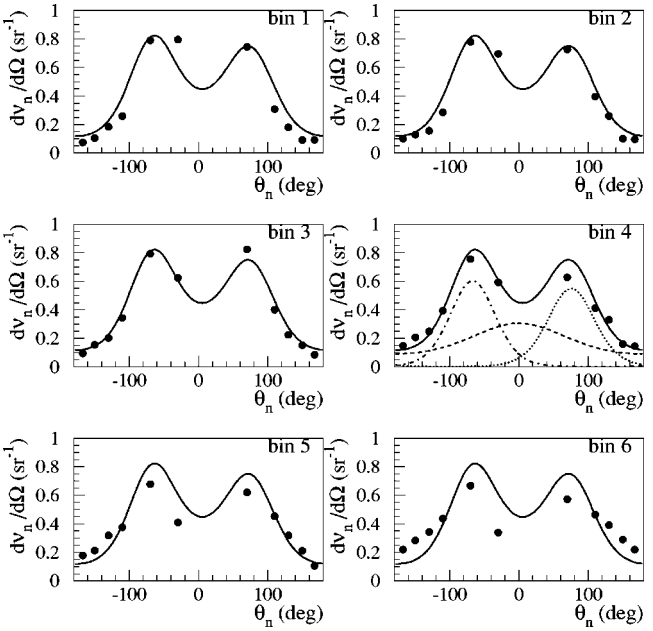

FIG. 7. Experimental angular distributions of the neutron multiplicities (solid circles) reconstructed for symmetric fission mass partition for various CN recoil-velocity bin selections (see Fig. 6). The distributions were obtained with the data collected in the $E=8$ MeV/nucleon ^{20}Ne+^{169}Tm reaction. The full curves represent the total contribution of the moving source fit to the data of bin 4. The other curves in bin 4 have the same meaning as in Fig. 2.

is still useful for determining their average velocities. However, the observed distribution width is not the real width of the velocity distribution of the nucleus that emitted the neutrons, because of these emissions.

Let us ignore this for the moment and make several bin cuts on the V_{CN} distribution. These cuts are numbered from 1 to 6 in Fig. 6. The bin widths for each cut were chosen in order to obtain comparable data statistics. For each cut, the experimental differential angular distributions of the neutron multiplicities $d\nu_n/d\Omega(\theta_n)$ were determined. They are displayed by the solid circles in Fig. 7 for the detectors set in the reaction plane ($\phi_n=0°$ and $\phi_n=180°$).

For bin 4, the closest value to the mean recoil velocity of the CN in Fig. 6, the energy and angular distributions were fitted in the manner discussed in Sec. II. No gates on mass-partition were made so the two postscission sources were assumed to have identical multiplicities and effective temperatures. The dashed curve represents the fit for the prescission neutron contribution, the dotted and dotted-dashed ones are those associated with the FFs, and the solid curve is the sum of these three contributions (no PE contribution). This last curve is to be compared with the experimental data (solid circles). We observe an excellent agreement. For the other bins, this total contribution curve is also shown and again should be compared to the corresponding experimental full points. Although at $E=8$ MeV/nucleon no incomplete fusion is contributing to the data [2], we clearly observe in Fig. 7 an apparent dependence of the angular distribution on the CN recoil-velocity. This behavior is due to the fact that the width of the recoil-velocity distribution is affected by the

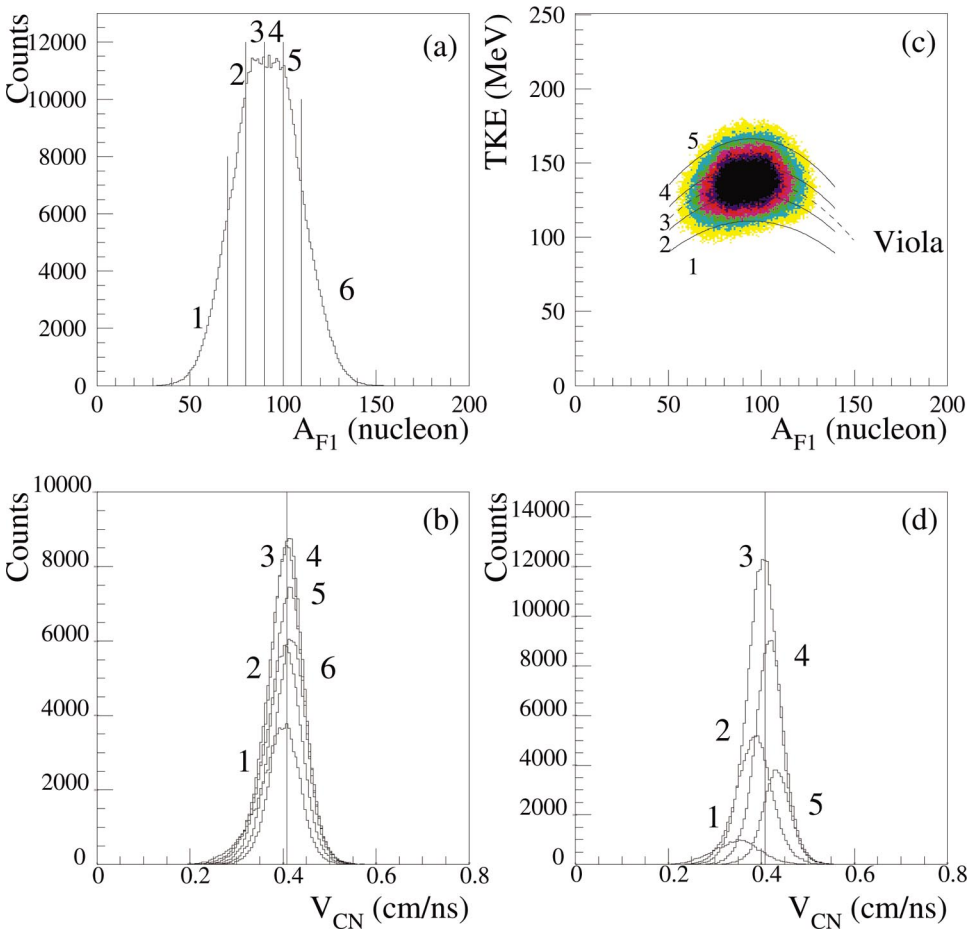

FIG. 8. (Color) (a) Fission-fragment mass A_{F1} distribution and (c) A_{F1}-TKE correlations extracted from the $E=8$ MeV/nucleon $^{20}Ne+^{169}Tm$ reaction with the Viola's prediction represented in dashed line; (b) V_{CN} distributions gated on the A_{F1} bins displayed in (a); (d) V_{CN} distributions gated on the two-dimensional gates displayed in (c).

recoil effects associated with evaporating these neutrons. Any constraint on the recoil velocity must bias the resulting distribution of these coincident neutrons.

In bin 6, to obtain the highest V_{CN} velocities, neutrons must be emitted at backward angles ($|\theta_n|>90°$). Compared to the solid curve for which V_{CN} is near its average value, the data in Fig. 7 (bin 6) show a strong enhancement for ($|\theta_n|>90°$). In contrast, the lowest V_{CN} velocities will boost the forward emissions as shown in Fig. 7 (bin 1). These observations lead to the conclusion that any cut on the V_{CN} distribution affects the observed isotropy, in their source frame, of the neutron emissions. Therefore the analysis method described in Sec. II and Ref. [2], which assumes this isotropy, is not anymore appropriate.

Now if we consider a reaction for which incomplete fusion is also significant, gating on the highest recoil velocities as in Refs. [14,15] might well remove the incomplete-fusion events, but the remaining complete-fusion events will still be biased. In the case of selecting higher than average recoil velocities, as in the bin 6 example, the extracted prescission particle multiplicity will be too large as this is the most important contribution at backward angles in the fits [see Fig. 2(b)]. It will be compensated by lower postscission multiplicities in order to fit the forward angles ($|\theta_n|<90°$). This situation is inverted if the low CN recoil velocities are selected.

Consequently, it is clear that selecting the highest CN recoil velocities to isolate the complete-fusion events in a given nuclear reaction, without taking into account the boost effects from the neutron emission, can lead to incorrect determination of the fitted neutron emission properties. This conclusion is due to the destruction of isotropy in the neutron emission from each of the three sources which is a fundamental hypothesis in the data analysis discussed in the previous section and most other analysis schemes.

B. Effects of the FF mass and TKE distributions on the fission neutron multiplicities

Given the problems that can be induced by gating on the recoil-velocity distributions, it is useful to consider whether gates on other fission parameters may induce similar effects. Let us consider selections on either the FF mass distribution or TKE distribution where we will again choose the data obtained with the $E=8$ MeV/nucleon $^{20}Ne+^{169}Tm$ reaction. Figure 8 shows how different cuts operated on the FF mass partition (left), and on TKE (right), modify the CN recoil-velocity distribution. Clearly, from Figs. 8(a) and 8(b), the CN recoil-velocity distributions are not affected by any FF mass selection. In fact, these distributions remain centered around the same V_{CN} maximum with approximately equal widths.

Figure 8(c) represents the bidimensional spectrum displaying the correlation between the measured TKE and A_{F1} observable. Gating on TKE, horizontal cuts in Fig. 8(c), result in different A_{F1} distributions for each gate. Hinde *et al.* [3] suggested gating on the related variable

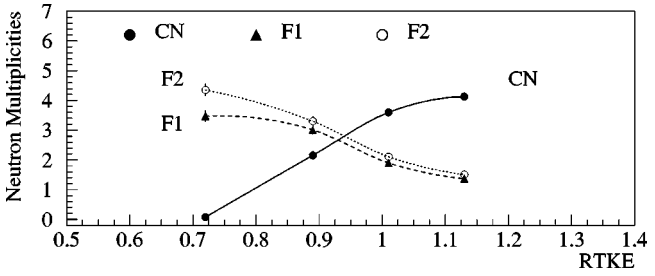

FIG. 9. Dependence of the extracted ν_n^{CN}, ν_n^{F1}, and ν_n^{F2} neutron multiplicities on the RTKE variable [see Fig. 8(c)] for the $E=8$ MeV/nucleon ^{20}Ne+^{169}Tm reaction (see text for details). Curves guide the eye.

$$\mathrm{RTKE} = \frac{\mathrm{TKE_{exp}}}{0.755 Z_1 Z_2/(A_1^{1/3}+A_2^{1/3})+7.3}, \qquad (11)$$

in order to ensure the A_{F1} distributions are approximately the same for each gate. The denominator of this relation is the semi-empirical expression of Viola [18] extended by Hinde *et al.* [10] to account for asymmetric mass partitions. Thus, RTKE=1 [corresponding to the dashed curve in Fig. 8(c)] represents the exact value of the Viola systematics. Using constant RTKE cuts, as shown in Fig. 8(c) (bin cuts 1–5), we build the corresponding V_{CN} distributions plotted in Fig. 8(d). Clearly, such selections on RTKE (without affecting the A_{F1} distribution) induce different V_{CN} distributions [labeled 1–5 in Fig. 8(d)] with different centroids and widths. In fact, one observes that the V_{CN} centroids move to higher values with increasing RTKE (from 0.7 to 1.15). As the CN recoil velocity is expected to be single valued, this dependence on RTKE is an artifact of the analysis and again must be related to a bias in the neutron emissions. Consequently if analyzed with the assumption of isotropic emission, it will clearly generate (as discussed in Sec. IV A) incorrect determinations of the neutron emission properties.

Indeed, Fig. 9 shows the results of the fitted neutron multiplicities as a function of the RTKE variable for the reaction $E=8$ MeV/nucleon ^{20}Ne+^{169}Tm. Obviously, we observe a nonphysical increase in the prescission multiplicities ν_n^{CN} with increasing RTKE values. This behavior is subsequently compensated by the decrease of the fitted ν_n^{F1} and ν_n^{F2} values.

The observation of similar spurious RTKE dependences has been made in Refs. [3,11]. Rossner *et al.* [19] have simulated neutron emission in the $E=5.7$ MeV/nucleon ^{36}Ar +^{169}Tm fission reaction without any intrinsic RTKE dependence and have shown that the standard analysis does lead to a spurious RTKE dependence similar to that obtained with their experimental data. Hinde *et al.* [3] introduce a recoil correction, involving a renormalization of the number of single fission events in the RTKE gate. However, the recoil corrections were not applied to the prescission source and accounted for only about 70% of the correlation with RTKE. The other 30% was assigned to "still uncorrected recoil effects" and it is there concluded that "further detailed investigation is required." We wish to emphasize that it is not only cuts on TKE that invalidate the conventional analysis of neutron angular correlations, but also cuts on V_{CN}. Indeed, analysis of neutron angular correlations with cuts on a parameter significantly affected by neutron evaporation will need the development of a more sophisticated analysis than has up to now been attempted.

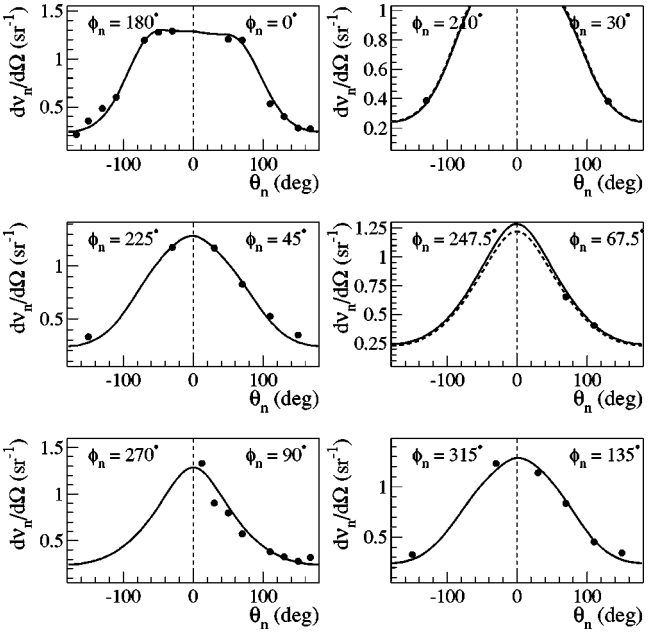

FIG. 10. Experimental neutron angular distributions extracted for the $E=16$ MeV/nucleon ^{20}Ne+^{169}Tm reaction. Distributions are shown for the reaction plane ($\phi_n=0°, 180°$) and the other indicated ϕ_n angles. For the reaction plane ($\phi_n=0°, 180°$) , the full curve is a fit to the plotted data. From this fit, the predicted distributions for the other ϕ_n planes are also indicated by full curves for comparison. In some ϕ_n planes, a small correction factor was applied to improve the comparison between the experimental points (solid circles) and these full lines. The resulting corrected angular distributions are shown as dashed lines (see plane $\phi_n=67.5°, 247.5°$ figure).

C. Isotropy of the neutron emissions in and out of the reaction plane and the parametrization of their out of plane angular distributions

In Ref. [5], it was shown, after a detailed analysis, that the neutron emission characteristics (ν_n^i and $T^i{}_n$) extracted from the fit of the data from all DEMON detectors ($0° \leqslant \phi_n < 360°$) were very close to those determined by fitting only the data for the detectors set in the reaction plane ($\phi_n=0°$ or $\phi_n=180°$). Following this observation, it was concluded that the CN angular momentum, perpendicular to the reaction plane, must not significantly affect the angular distribution of the neutron emission.

In order to investigate this assumption more deeply, a fit to the neutron angular distribution $d\nu_n/d\Omega$ was performed for the reaction ^{20}Ne+^{169}Tm at $E=16$ MeV/nucleon using only the detectors in the reaction plane ($\phi_n=0°$ or $\phi_n=180°$). The parameters extracted from this fit (ν_n^i and $T^i{}_n$) were then applied to predict the distributions out of the reaction plane for isotropic emission. These distributions (solid curves) are presented in Fig. 10 and compared to the experimental values (solid circles). For the dashed curves, empiri-

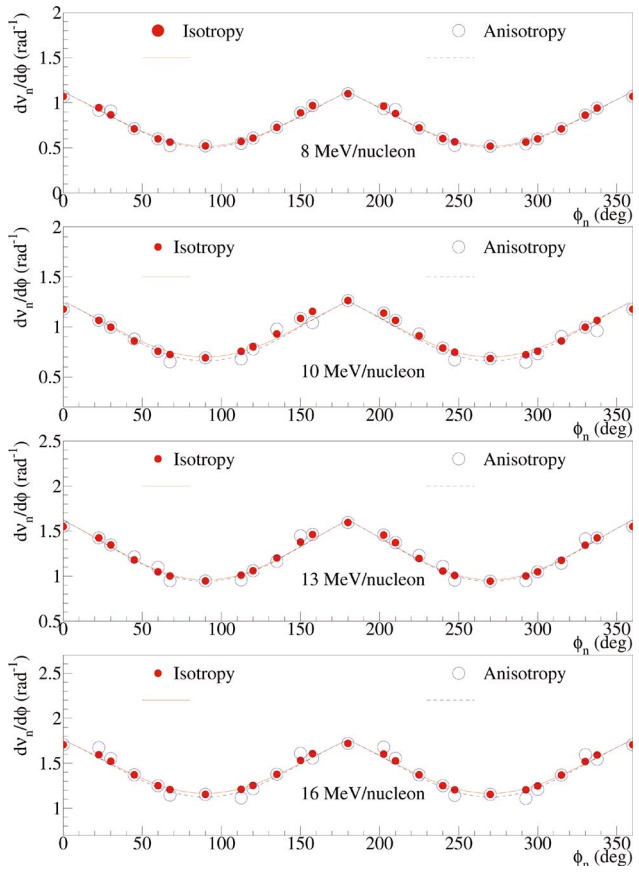

FIG. 11. (Color) Results of the neutron emission isotropy and/or anisotropy in and out of the reaction plane for the reaction ^{20}Ne $+^{169}$Tm at the four bombarding energies (see text for details). The solid lines represent the results of the best fits to the solid circles using Eq. (13). The dashed lines result from fits to the corrected data (open circles) using Eq. (14).

cal normalization factors (see below) were applied on these curves to achieve, when needed, the best comparison with each experimental distribution. One can directly observe that these correction factors are very small and had to be applied for only few ϕ_n planes. In fact, the results without correction can already be considered as relatively good.

This study was extended by integrating, over θ_n angles, Eq. (6) with and without the correction factors, i.e.,

$$\frac{d\nu_n}{d\phi}(\phi_n) = \int_0^{\pi} \frac{d\nu_n}{d\Omega}(\theta_n, \phi_n)\sin(\theta_n)d\theta_n. \qquad (12)$$

The results of these integrations are plotted in Fig. 11 for the ^{20}Ne$+^{169}$Tm reaction at the four projectile energies.

In Fig. 11, the solid circles represent the ϕ_n evolutions of $d\nu_n/d\phi$ without corrections. The results with corrections are represented by the open circles. In principle, any observed difference between these two sets of data points suggests the occurrence of an anisotropy in the neutron emission in and out of the reaction plane. For each bombarding energy, the solid lines are the results of the best fit to the solid circles data using the following expression

TABLE II. Values of the parameters obtained from the fitting neutron angular distribution $d\nu_n/d\phi(\phi_n)$ (see Fig. 11) by Eqs. (13) and (14) for the ^{20}Ne$+^{169}$Tm reaction at the four bombarding energies (see text for details).

Reactions	A	B	C	D
Tm08	2.299	−1.175	0.414	0.009
Tm10	2.334	−1.075	0.419	0.023
Tm13	2.810	−1.186	0.446	0.008
Tm16	2.810	−1.050	0.449	0.024

$$\frac{d\nu_n}{d\phi} = A + B\,\exp(C\,\sin(\phi_n)), \qquad (13)$$

where A, B, and C are free parameters. This expression is suggested by Eq. (4). The values resulting from these fits are listed in Table II. The dashed lines in Fig. 11 result from fits to the corrected data (open circles) by similar equation, but with an extra $\exp(D\,\sin^2(\phi_n))$ term. The resulting function can thus be written

$$\frac{d\nu_n}{d\phi} = A + B\,\exp[C\,\sin(\phi_n) + D\,\sin^2(\phi_n)]. \qquad (14)$$

In this case D is the only parameter to be adjusted, i.e., the values of the parameters A, B, and C are held fixed at their values obtained in the original fit with Eq. (13). The four parameters, extracted from both fits, are listed in Table II.

Following our approach, the correction factor $\exp(D\,\sin^2(\phi_n))$ accounts for the anisotropy of the angular distribution of the neutron emission out of the reaction plane compared with emission in the reaction plane. Still, with the experimentally extracted small D values, one does not have to justify any important anisotropy in the neutron emission out of the reaction plane even at $\phi_n = 90°$. One must notice that the integrations of Eqs. (13) and (14) give the neutron multiplicities displayed in Fig. 5.

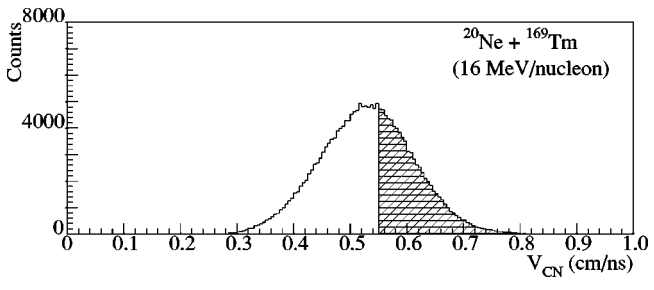

FIG. 12. Extracted recoil-velocity (V_{CN}) distribution for the $E = 16$ MeV/nucleon ^{20}Ne$+^{169}$Tm reaction. The shaded area represents the selection on the velocities higher than 90% of the CN recoil velocity expected for complete fusion.

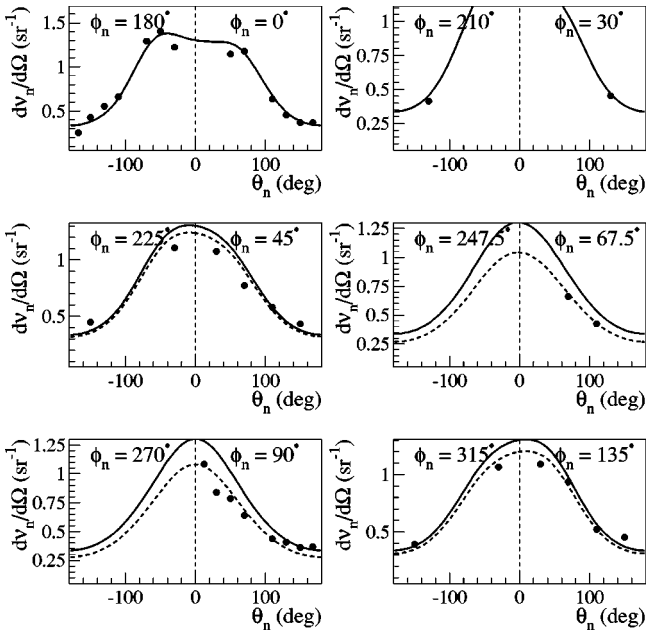

FIG. 13. Same as Fig. 10 after the selection of the highest values of V_{CN} recoil-velocities as shown in Fig. 12.

D. Effects of the CN recoil velocity on the neutron emission in and out of the reaction plane (confirmation of Sec. IV A conclusion)

It is of interest to go back to the CN recoil-velocity distribution and investigate any V_{CN} effect on the neutron emission isotropy. In fact, if a given selection on the CN recoil velocity destroys the isotropy of the neutron emission (see the conclusions of Sec. IV A), we should be able to observe this effect in such an analysis. In order to investigate this, we have applied such an analysis on the data of the $E=16$ MeV/nucleon ^{20}Ne+^{169}Tm reaction selecting higher values of V_{CN}, larger than 90% of the expected value for complete fusion as shown in Fig. 12. Such a selection could in principle be applied in order to isolate complete-fusion events. The consequences of this selection on the neutron angular distributions in and out of the reaction plane are shown in Fig. 13.

The same procedure as in Fig. 10 and Sec. IV B was followed resulting in the anisotropy displayed in Fig. 14. If we compare Figs. 13 and 10 for the reaction plane ($\phi_n=0°$ and 180°), the selection of the high component of the CN recoil-velocity distribution leads to an important increasing of the neutron yields at backward angles ($|\theta_n|>90°$). In order to fit these data points, the prescission neutron multiplicity has to be artificially increased. In contrast, the postscission neutron multiplicities must be artificially decreased. This effect was already discussed in Sec. IV A. Figure 14 should be compared to Fig. 11 for the $E=16$ MeV/nucleon data. One observes that the behavior of the open circles, displaying the induced anisotropy of the neutron emission out of the reaction plane, is still very close to the original behavior in Fig. 11 without any V_{CN} gate. In contrast for the solid circles constructed with the assumption of isotropic neutron emission, the $d\nu_n/d\phi(\phi)$ distribution is more flat

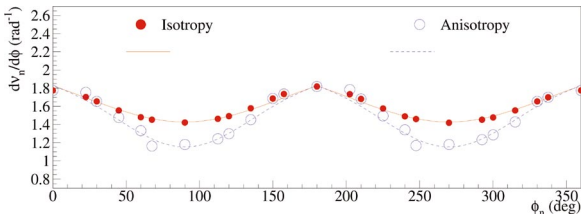

FIG. 14. (Color) Same as Fig. 11 just for the $E=16$ MeV/nucleon reaction after the selection of the highest values of the CN recoil-velocities shown in Fig. 12.

and strongly overestimates the values at the planes $\phi_n=90°$ and 270° where the prescission neutron emission dominates.

These figures clearly show that any selection applied to the CN recoil-velocity affects the isotropy of the neutron emission in fusion-fission reactions such as ^{20}Ne+^{159}Tb and ^{20}Ne+^{169}Tm between $E=8$ and 16 MeV/nucleon, and especially for the prescission neutron emission which dominates around $\phi_n=90°$. With this V_{CN} gate, the formalism used to extract multiplicities and effective temperatures is completely inappropriate.

V. CONCLUSION

Neutron emission in $E=8$, 10, 13, and 16 MeV/nucleon ^{20}Ne+^{159}Tb and ^{20}Ne+^{169}Tm induced fission reactions have been studied. The 4π configuration of the DEMON neutron multidetector setup allowed us to investigate, with high statistics and good granularity, the properties of neutron emission in and out of the reaction plane and as functions of the fission mass partition, the total kinetic-energy release in fission TKE, and the recoil velocity V_{CN} of the compound nucleus. For the reactions studied, the isotropy of the neutron evaporation in the rest frame of the emitting nucleus was clearly demonstrated. Within the experimental uncertainties, the extracted total neutron multiplicity was found to be independent of the fission fragment mass partition. In contrast, the prescission neutron multiplicity appeared to be slightly dependent showing a smaller value for the most asymmetric partition. The extracted postscission neutron multiplicities were found to increase roughly linearly with fragment mass as expected if the fission fragments, in all mass partitions, have a common temperature.

The determination of the compound-nucleus recoil velocity and the kinetic-energy release in fission suffer from smearing due to the recoil kicks imparted by the evaporated pre- and postscission light particles. Any selection gating on the reconstructed quantities can impart a bias in the emission pattern of these evaporated particles. Such effects were observed for the recoil velocity and the kinetic-energy release in fission as the emission of the evaporated particles displays an apparent anisotropy in their emitter frame. Analysis of such gated neutron data with the standard method which assumes isotropy, results in spurious dependences of the extracted multiplicities on TKE and V_{CN}. For the mass-partition, these biases were found to be nonexistent.

ACKNOWLEDGMENTS

The authors are indebted to the crew of Louvain-la-Neuve Cyclotron for the excellent and efficient running of the machine. We also thank Mr. P. Demaret for his important contributions to the target preparation. Some of us (R.J.C., J.B.N., and D.J.H.) would like to thank the University of Louvain for its hospitality during their multiple stays in Belgium.

[1] D. Hilscher and H. Rossner, Ann. Phys. (Paris) **17**, 471 (1992), and references therein.
[2] J. Cabrera, T. Keutgen, Y. El Masri, C. Dufauquez, V. Roberfroid, I. Tilquin, J. Van Mol, R. Régimbart, R. J. Charity, J. B. Natowitz, K. Hagel, R. Wada, and D. J. Hinde, Phys. Rev. C **68**, 034613 (2003).
[3] D. J. Hinde, D. Hilscher, H. Rossner, B. Gebauer, M. Lehmann, and M. Wilpert, Phys. Rev. C **45**, 1229 (1992).
[4] I. Tilquin *et al.*, Nucl. Instrum. Methods Phys. Res. A **365**, 446 (1995).
[5] Th. Keutgen, Ph.D. thesis, Université Catholique de Louvain, 1999.
[6] K. J. LeCouteur and D. W. Lang, Nucl. Phys. **13**, 32 (1959).
[7] D. W. Lang, Nucl. Phys. **53**, 113 (1964).
[8] J. B. Cabrera, Ph.D. thesis, Université Catholique de Louvain, 2002.
[9] D. J. Hinde, H. Ogata, M. Tanaka, T. Shimoda, N. Takahashi, A. Shinohara, S. Wakamatsu, K. Katori, and H. Okamura, Phys. Rev. C **39**, 2268 (1989).
[10] D. Hinde, J. Leigh, J. Bokhorst, J. Newton, R. Walsh, and J. Boldeman, Nucl. Phys. **A472**, 318 (1987).
[11] H. Rossner, D. Hilscher, D. J. Hinde, B. Gebauer, M. Lehmann, M. Wilpert, and E. Mordhorst, Phys. Rev. C **40**, 2629 (1989).
[12] R. J. Charity, Phys. Rev. C **51**, 217 (1995).
[13] J. Newton, D. Hinde, R. Charity, J. Leigh, J. Bokhorst, A. Chatterjee, G. Foote, and S. Ogaza, Nucl. Phys. **A483**, 126 (1988).
[14] E. Holub, D. Hilscher, G. Ingold, U. Jahnke, H. Orf, and H. Rossner, Phys. Rev. C **28**, 252 (1983).
[15] D. Hilscher *et al.*, Phys. Rev. C **36**, 208 (1987).
[16] E. Mordhorst, M. Strecker, H. Frobeen, M. Gasthuber, W. Scobel, B. Gebauer, D. Hilscher, M. Lehmann, H. Rossner, and W. Wilpert, Phys. Rev. C **43**, 716 (1991).
[17] K. Knoche, L. Lüdemann, W. Scobel, B. Gebauer, D. Hilscher, D. Polster, and H. Rossner, Phys. Rev. C **51**, 1908 (1995).
[18] V. E. Viola, K. Kwiatkowski, and M. Walker, Phys. Rev. C **31**, 1550 (1985).
[19] H. Rossner, D. Hilscher, and D. Hinde, Phys. Rev. C **43**, 2434 (1991).